PHYSICAL REVIEW B VOLUME 52, NUMBER 21 1 DECEMBER 1995-I

Features of a eutectoid reaction in a Ti–40 at. % Al alloy: Evidence for an amorphous-state formation from a crystal

M. Tanimura and Y. Inoue
Structural Analysis Section, Research Department, Nissan ARC Ltd., 1 Natsushima-cho, Yokosuka 237, Japan

Y. Koyama
Kagami Memorial Laboratory for Materials Science and Technology and Department of Materials Science and Engineering, Waseda University, Shinjuku-ku, Tokyo 169, Japan

(Received 20 June 1995)

In an initial stage of a eutectoid reaction of a Ti–40 at. % Al alloy, hcp→$D0_{19}+L1_0$, an amorphous state was found to form around an intermediate precipitate with the B_{19} structure, together with a change in crystal structure of the matrix from the hcp structure to the $D0_{19}$ one. Characteristic features of the amorphous state are that the destruction of the crystal lattice mainly takes place in the (001) plane of the $D0_{19}$ structure but is very slightly extended along the [001] direction. The shape of the amorphous region is just like a thin film. On the basis of the present data, the origin of the two-dimensional-like character of the lattice destruction is simply discussed.

I. INTRODUCTION

The formation of an amorphous state from a crystal is one of the most fascinating phenomena in solid state physics from the viewpoint of the destruction of a crystal lattice. The amorphous state produced from a crystal has so far been obtained by some artificial techniques such as the gas-freezing method and ion irradiation.[1–8] As an equilibrium transition, however, a crystal-to-amorphous transition referred to as inverse melting was recently discussed theoretically by Greer[9] and actually found in the Ti-Cr alloy by Yan *et al.*[10] In addition to the inverse melting, we have very recently found the formation of an amorphous state in the initial stage of a eutectoid reaction of a Ti–40 at. % Al alloy. The details of the experimentally obtained data will be described below.

In the phase diagram of the Ti-Al alloy system, the eutectoid reaction from α to $\alpha_2+\gamma$ takes place around 1398 K at a composition of about 40 at. % Al. Note that the α, α_2, and γ phases have the hcp, $D0_{19}$, and $L1_0$ structures, respectively. From these structures, the reaction is understood to involve both a phase separation and an ordering. According to recent work on Ti–(38–48) at. % Al alloys, an α_2/γ lamellar structure has been found experimentally.[11–18] Because alloys having the lamellar structure exhibit good mechanical properties, the details of the lamellar structure have been extensively investigated for industrial application.[19,20] In this situation, we have examined features of the eutectoid reaction in the Ti–40 at. % Al alloy by transmission electron microscopy in order to understand the mechanism of formation of the lamellar structure. As a result, we found that the reaction proceeds via the formation of the amorphous state in the initial stage. In this paper, we describe experimental data on amorphous-state formation in the eutectoid reaction of the Ti–40 at. % Al alloy.

II. EXPERIMENTAL PROCEDURE

A sample preparation of the Ti–40 at. % Al alloy was made in the following way. An alloy ingot made by an Ar arc-melting technique was first annealed at 1523 K for 24 h for homogenization. In order to examine the change in microstructures during the eutectoid reaction, we prepared samples with four different aging times. The samples, with a size of $3\times5\times10$ mm^3, cut from the ingot were actually aged at 1273 K for 15 min, 25 min, 2 h, and 100 h, respectively, followed by quenching into ice water. The observation of microstructures was carried out at room temperature using an H-800 transmission electron microscope. Specimens for observation were mainly made by Ar-ion thinning after cutting the samples into disks 30 μm thick and with 1.5 mm radius. Some specimens were also prepared by electropolishing the samples in a solution of 10% $HClO_4$ in methanol.

The observation was made by taking electron diffraction patterns, both bright- and dark-field images. In particular, we observed samples involving the amorphous state in the following way. Diffraction patterns of the sample with the amorphous state consist of not only fundamental and superlattice spots due to the $D0_{19}$ and $L1_0$ structures but also halo rings due to the amorphous state. In order to obtain a conspicuous contrast due to the amorphous state, bright-field images were taken by using both the first halo ring and the diffraction spots inside the ring in diffraction patterns, not only a direct spot. As for dark-field images, we took images using part of the first halo ring to examine features of the amorphous state, in addition to ordinary dark-field images.

III. EXPERIMENTAL RESULTS

When the sample was kept at 1273 K below a eutectoid line of about 1398 K, the reaction from α to $\alpha_2+\gamma$ took place. Figure 1 shows two bright-field images taken from the samples aged for 2 and 100 h, respectively. Electron incidence for both images is parallel to the $[11\bar{2}]_{\alpha_2}$ direction where the subscript α_2 denotes the α_2 phase with the $D0_{19}$ structure. In the images, there exists a lamellar structure consisting of two regions; that is, a major region marked by A and a minor one by B. The lamellar structure is thus under-

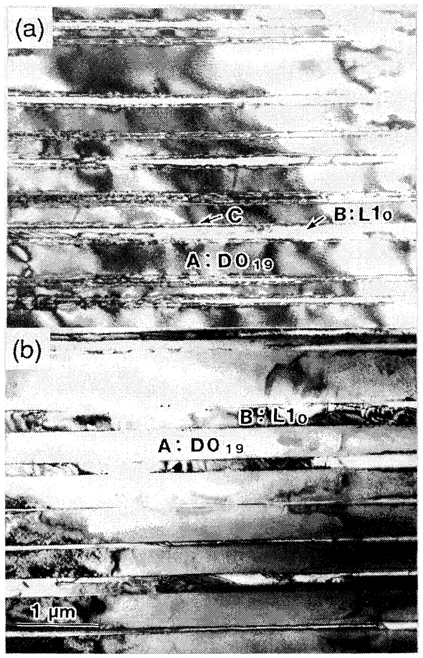

FIG. 1. Bright-field images taken from the samples aged at 1273 K for 2 h (a) and 100 h (b).

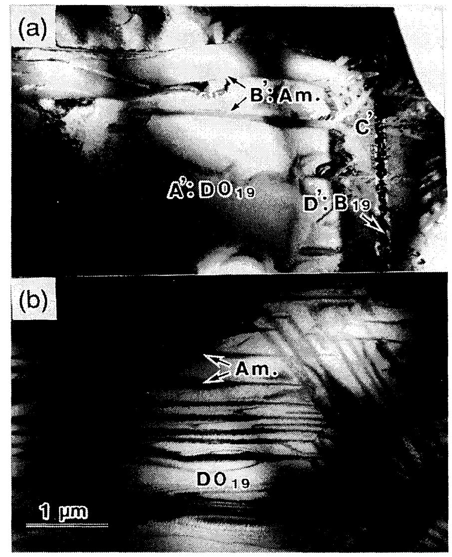

FIG. 2. Bright-field images taken from two different areas of the sample aged at 1273 K for 15 min. In these images, "Am." denotes the amorphous phase.

stood to be sufficiently developed within 2 h. A feature of the lamellar structure is that a complicated contrast is seen along the boundary between the major and minor regions only in the sample aged for 2 h, as indicated by the arrow C in Fig. 1(a). In order to examine the crystal structures of these regions, we took dark-field images using fundamental spots due to the $D0_{19}$ and $L1_0$ structures. From the images obtained, the major and minor regions in the samples were, respectively, confirmed to have the $D0_{19}$ and $L1_0$ structures as an equilibrium state. In the sample aged for 2 h, on the other hand, the complicated-contrast region in the bright-field image did not give rise to a bright contrast in dark-field images. In other words, the boundary region has an unknown structure. Because the complicated contrast along the boundary disappears in the sample aged for 100 h, Fig. 1(b), the existence of the complicated-contrast region must be a key factor to understanding the change in microstructures during the eutectoid reaction of the Ti–40 at. % Al alloy.

In order to examine the details of the boundary contrast found in the sample aged for 2 h, the observation of microstructures in the initial stage of the reaction was performed. Two bright-field images taken from two different areas in the sample aged for 15 min are shown in Fig. 2. Electron incidence for the images is parallel to the $[11\bar{2}]_{\alpha_2}$ direction. As can be seen in Fig. 2(a), there are four types of regions, A', B', C', and D', in the image. That is, in a matrix marked by A', two regions indicated by B' and C' appear around a region D' with an average width of about 200 nm, which gives rise to a deep dark band contrast with zigzag boundaries. An important feature of this microstructure is that the region B' exhibits an extremely uniform and featureless contrast like a liquid state. It is also worth noticing that features of the contrast in the region C' basically resemble those in the region B'. In Fig. 2(b), on the other hand, we can see a microstructure consisting of the featureless-contrast region and the matrix, which can be identified as a lamellar structure. From a comparison between Figs. 2(a) and 2(b), it seems that in the initial stage the featureless-contrast region B' is nucleated in the C' regions, grows at the expense of the matrix, and the lamellar structure is then formed.

Crystal structures of the four regions in Fig. 2(a) were determined by taking both electron diffraction patterns and dark-field images. Figure 3(a) is an electron diffraction pattern with incidence parallel to the $[11\bar{2}]_{\alpha_2}$ direction, which was obtained from the area shown in Fig. 2(a). From a simple analysis of the pattern, both diffraction spots due to the $D0_{19}$ structure and a halo ring are found to exist. Features of the pattern are that only the first halo ring is detected and the distance between the origin 000 and the ring corresponds to the (111) interplanar spacing of the γ phase. Then, we first took a dark-field image by using the 222 fundamental spot due to the $D0_{19}$ structure, Fig. 3(b). In the image, the regions A' and C' in Fig. 2(a) give rise to a bright contrast, while small regions observed as a dark contrast are involved in the region C'. This means that the crystal structure of the matrix A' in Fig. 2(a) has the $D0_{19}$ structure, which is identical to that of the major region A in Fig. 1. That is, a change in the structure of the matrix from the hcp structure to the $D0_{19}$ one takes place in the initial stage of the reaction. As for the region D', its crystal structure was confirmed to be the B_{19} structure from other diffraction patterns with different incidences, as was analyzed by Takeyama for Ti–48 at. % Al alloys.[21]

In order to understand the structures of the regions B' and C', we tried to take a dark-field image [Fig. 3(c)] using a part of the first halo ring, which is indicated by a square in Fig. 3(a). Surprisingly, a bright contrast is obtained in the regions B' and C'. This obviously indicates that the amorphous state appears in the initial stage of the reaction. That is, the fea-

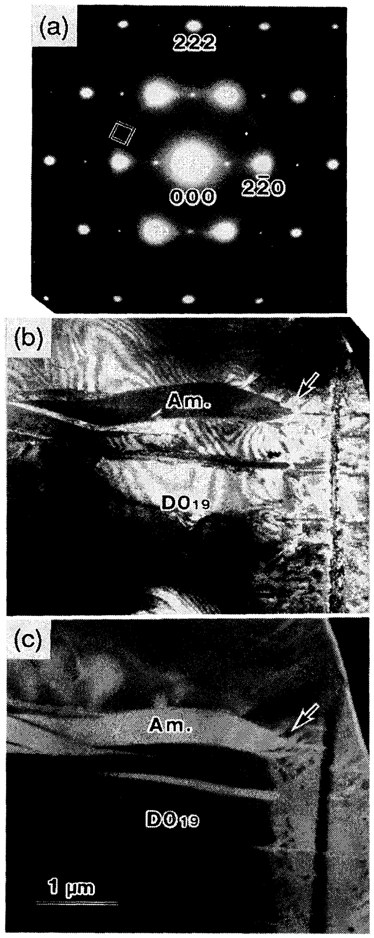

FIG. 3. Electron diffraction pattern (a) and dark-field images (b) and (c), which were obtained from the area shown in Fig. 2(a). In the pattern, diffraction spots are indexed in terms of the $D0_{19}$ structure. The dark-field images were, respectively, taken by using the 222 fundamental spot due to the $D0_{19}$ structure (b), and a part of the first halo ring (c).

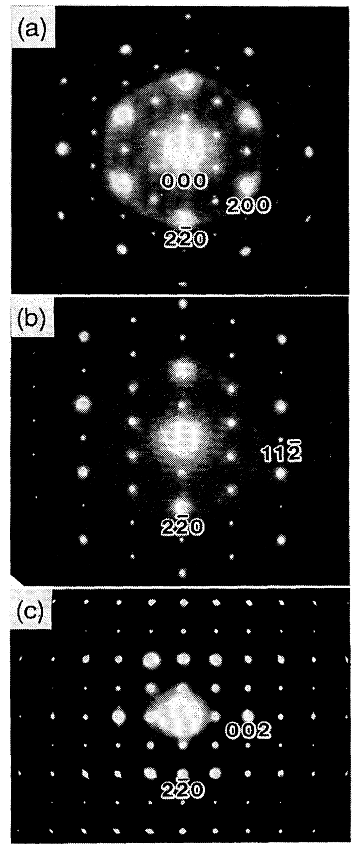

FIG. 4. Electron diffraction patterns taken from the same area in the sample aged for 15 min. The electron incidences are parallel to the $[001]_{\alpha_2}$ (a), $[111]_{\alpha_2}$ (b), and $[110]_{\alpha_2}$ directions (c).

tureless contrast in the bright-field image, the region B', really originates from the amorphous state. In the region C', because dark-contrast regions in Fig. 3(c) basically correspond to the bright-contrast regions in Fig. 3(b), as indicated by arrows, the $D0_{19}$ crystalline and amorphous states are understood to coexist. In addition to these features, the region B' is observed as band- and needle-like shapes along the $\langle 110\rangle_{\alpha_2}$ directions in the images. From this fact, it seems that the amorphous regions grow along these directions.

The above-mentioned data indicate that the amorphous state appears in the initial stage of the eutectoid reaction. In order to obtain a basic understanding of the nature of the amorphous state, we examined the change in intensity of the first halo ring when a sample is rotated. Figure 4 shows a series of electron diffraction patterns obtained from a region with the amorphous and $D0_{19}$ structures in the sample aged for 15 min. Note that the sample was rotated from the $[001]_{\alpha_2}$ direction to the $[110]_{\alpha_2}$ one in the present experiment. Electron incidences of Figs. 4(a), 4(b), and 4(c) are parallel to the $[001]_{\alpha_2}$, $[111]_{\alpha_2}$, and $[110]_{\alpha_2}$ directions, respectively. In the $[001]_{\alpha_2}$ direction, Fig. 4(a), there is the first halo ring with the strongest intensity in the pattern. When the sample is rotated from the $[001]_{\alpha_2}$ direction, the intensity continuously decreases, as seen in Figs. 4(b) and 4(c). Actually the pattern with the incidence in the $[110]_{\alpha_2}$ direction, Fig. 4(c), exhibits the weakest intensity. From this fact, the intensity is understood to have a strong dependence on the sample orientation. This obviously indicates that the destruction of the crystal lattice takes place mainly in the $(001)_{\alpha_2}$ plane but is very slightly extended along the $[001]_{\alpha_2}$ direction. That is, the amorphous state found in the initial stage of the eutectoid reaction in the Ti–40 at. % Al alloys has two-dimensional-like character. In other words, the amorphous region has a shape like a thin film, the normal axis of which is parallel to the $[001]_{\alpha_2}$ direction. It should be remarked that the two-dimensional-like character never means a two-dimensional destruction. The destruction actually has a three-dimensional nature with a strong anisotropy. Eventually, the change in the intensity of the halo ring is concluded to arise from the geometry of the volume occupied by the amorphous state.

To understand the relation between the microstructures of the samples aged for 15 min and 2 h, we next examined the microstructure of a sample aged for 25 min by taking bright- and dark-field images. In this experiment, we also checked

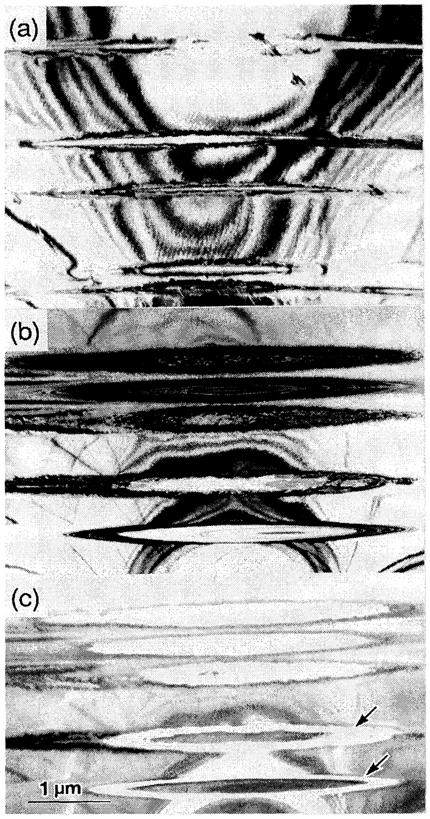

FIG. 5. Bright-field images (a) and (b) and dark-field image (c) of the samples aged for 25 min. Among these images, the two bright-field images were taken from samples made by ion thinning (a) and electropolishing (b). The dark-field image (c) was also taken from the area shown in (b), by using a part of the first halo ring.

the effect of the Ar-ion thinning in the sample preparation on microstructures appearing during the eutectoid reaction. Figures 5(a) and 5(b) are bright-field images of samples aged for 25 min, which were prepared by ion thinning and electropolishing, respectively. Electron incidence for these images is parallel to the $[11\bar{2}]_{\alpha_2}$ direction. From these images, the microstructure shown in Fig. 5(a) is found to be almost identical to that in Fig. 5(b). That is, lenticular-shape precipitates are observed in these images. A feature of the lenticular-shape precipitates is that a complicated contrast is detected along the boundary between the matrix and the precipitates. Because an analysis of corresponding diffraction patterns indicates that the matrix and the precipitate have the $D0_{19}$ and $L1_0$ structures, respectively, this microstructure is the same as that in the sample aged for 2 h, Fig. 1(a). It is also worth noticing that there exists the first halo ring with weak intensity in the diffraction patterns. We then tried to take dark-field images using a part of the ring. Figure 5(c) is a halo dark-field image obtained from the sample made by electropolishing. Although a bent contour is seen in the matrix, the boundary region gives rise to a bright contrast, as indicated by arrows. This means that the amorphous state exists along the boundary region observed as a complicated contrast. In other words, the amorphous state appearing in the initial stage starts to crystallize into the $L1_0$ structure inside the precipitate on aging for 25 min. In addition, this also indicates that the complicated-contrast region C in Fig. 1(a) should be due to the amorphous state. That is, the amorphous state still exists along the boundary between the precipitate and the matrix in the middle stage of the eutectoid reaction. It should be further remarked that the three lenticular-shape precipitates observed in the upper part of Fig. 5(c) exhibit a different contrast from the two precipitates in the lower part. In particular, the boundary region in the upper precipitates gives rise to a dark contrast, unlike the bright contrast in the lower ones. Because a bent contour is seen in the matrix, the difference in the contrast is presumably due to that in the Bragg condition. Therefore we believe that there is basically no difference among the microstructures of these five lenticular-shape precipitates.

As for the effect of ion thinning, we pay attention to the fact that the microstructure in Fig. 5(a) is essentially identical to that in Fig. 5(b), as was described above. That is, the ion thinning does not produce any change in the microstructure at all. It is then understood that the amorphous state is not induced by the ion thinning in the sample preparation but actually appears in the initial stage of the eutectoid reaction of the Ti–40 at. % Al alloy.

IV. DISCUSSION

From the above-mentioned results, the eutectoid reaction in the Ti–40 at. % Al alloy can be explained in the following scenario. When the sample is aged at 1273 K, the precipitate with the B_{19} structure first appears, together with a change in the crystal structure of the matrix from the hcp structure to the $D0_{19}$ one. The appearance of the B_{19} precipitate then produces the amorphous state, the regions B' and C' in Fig. 2(a), around it. On further aging, although both the B_{19} precipitate and the amorphous region C' disappear, the amorphous region observed as the region B' in Fig. 2(a) grows along one of the $\langle 110\rangle_{\alpha_2}$ directions and the lamellar structure consisting of the $D0_{19}$ and amorphous regions is then developed. In the middle and later stages corresponding to aging for more than 25 min, the amorphous state is crystallized into the $L1_0$ structure. Because the crystallization takes place inside the amorphous region, the complicated contrast along the boundary in the samples aged for 25 min and 2 h is eventually understood to be due to the amorphous state.

Let us simply discuss the origin of the formation of the amorphous state in the initial stage of the reaction in the Ti–40 at. % Al alloy. From the present data, the amorphous state is understood to be induced by the appearance of the B_{19} precipitate in the $D0_{19}$ matrix. Note that the $D0_{19}$ and B_{19} structures have stoichiometric concentrations of 25 and 50 at. % Al, respectively. Because the present alloy has 40 at. % Al, vacancies should occupy 50% of the Ti sites in the $D0_{19}$ structure if the deviation from stoichiometry is compensated by only vacancies. It is obvious that this estimation for the vacancy concentration is not true. A lot of Al atoms must occupy the Ti sites in order to stabilize the $D0_{19}$ structure. In this situation, we should imagine the appearance of the B_{19} precipitate with 50 at. % Al in the $D0_{19}$ matrix. The precipitation removes Al atoms from the Ti and Al sites in the $D0_{19}$ matrix around the precipitate. The removal of the Al atoms leads to an increase in the vacancy concentration of the matrix, so that the crystal lattice of the $D0_{19}$ structure cannot be stabilized beyond a critical concentration of vacancies. In other words, the amorphous state is realized in a real system. In the present work, unfortunately, it is impossible to estimate either the vacancy concentration in the $D0_{19}$ area before the appearance of the B_{19} precipitate or the critical concentration experimentally.

The amorphous state has a two-dimensional-like character. That is, the destruction of the crystal lattice mainly takes place in the $(001)_{\alpha_2}$ plane but is very slightly extended along the $[001]_{\alpha_2}$ direction. According to previous work on the α_2/γ lamellar structure in Ti-Al alloys,[11] it was found that the $(001)_{\alpha_2}$ plane is parallel to the $(111)_\gamma$ one and the interplanar spacing of the $(002)_{\alpha_2}$ plane is very close to that of the $(111)_\gamma$ one. In addition, the present work shows that the amorphous state, which changes into the $L1_0$ structure on aging, is produced by the appearance of the B_{19} precipitate in the $D0_{19}$ matrix. From these facts, it is possible that the structural change from the $D0_{19}$ structure to the $L1_0$ one takes place only by the rearrangement of atoms in the $(001)_{\alpha_2}$ plane. In other words, diffusion along the $[001]_{\alpha_2}$ direction does not necessarily occur during the structural change. It is further known that diffusion is very easy in the amorphous state, not in an ordered lattice. On the basis of this speculation, the two-dimensional-like character of the lattice destruction is understood to be an effort of the alloy toward phase separation in the ordered lattice, which actually occurs during the eutectoid reaction of the Ti–40 at. % Al alloy.

ACKNOWLEDGMENTS

The authors would like to thank Professor M. Kikuchi and Professor M. Takeyama, Tokyo Institute of Technology, very much for a useful discussion concerning this matter.

[1] B. X. Liu, W. L. Johnson, and M.-A. Nicolet, Appl. Phys. Lett. **42**, 45 (1983).
[2] B. Y. Tsaur, S. S. Lau, and J. W. Meyer, Appl. Phys. Lett. **36**, 823 (1980).
[3] H. Mori, H. Fujita, M. Tendo, and M. Fujita, Scr. Metall. **18**, 783 (1984).
[4] D. E. Luzzi, H. Mori, H. Fujita, and M. Meshii, Scr. Metall. **19**, 897 (1985).
[5] Y. Limoge and A. Barbu, Phys. Rev. B **30**, 2212 (1984).
[6] K. Aoki, X-G. Li, and T. Masumoto, Acta Metall. Mater. **40**, 1717 (1992).
[7] K. Aoki, X-G. Li, T. Hirata, E. Matsubara, Y. Waseda, and T. Masumoto, Acta Metall. Mater. **41**, 1523 (1993).
[8] R. B. Schwarz and W. L. Johnson, Phys. Rev. Lett. **51**, 415 (1983).
[9] A. L. Greer, J. Less-Common Met. **140**, 327 (1988).
[10] Z. H. Yan, T. Klassen, C. Michaelsen, M. Oehring, and R. Bormann, Phys. Rev. B **47**, 8520 (1993).
[11] M. J. Blackburn, in *Technology and Application of Titanium*, edited by R. T. Jaffee and N. E. Promisel (Pergamon, London, 1970), p. 633.
[12] C. R. Feng, D. J. Michel, and C. R. Crowe, Scr. Metall. **22**, 1481 (1988); **23**, 1135 (1989); Philos. Mag. Lett. **61**, 95 (1990).
[13] D. S. Schwartz and S. M. L. Sastry, Scr. Metall. **23**, 1621 (1985).
[14] H. Inui, A. Nakamura, M. H. Oh, and M. Yamaguchi, Ultramicroscopy **39**, 268 (1991).
[15] G. J. Mahon and J. M. Howe, Metall. Trans. **21A**, 1655 (1990).
[16] G. Hug, A. Loiseau, and P. Veyssiere, Philos. Mag. A **57**, 499 (1988).
[17] C. L. Fu and M. H. Yoo, Philos. Mag. Lett. **62**, 159 (1990).
[18] C. Woodward, J. M. MacLaren, and S. Rao, in *High-Temperature Ordered Intermetallic Alloys IV*, edited by L. A. Johnson, D. P. Pope, and J. O. Stieler (Materials Research Society, Pittsburgh, 1991), p. 125.
[19] D. Shechtman, M. J. Blackburn, and H. A. Lipsitt, Metall. Trans. **5**, 1373 (1974).
[20] E. L. Hall and S. C. Huang, J. Mater. Res. **4**, 595 (1989).
[21] M. Takeyama (private communication).

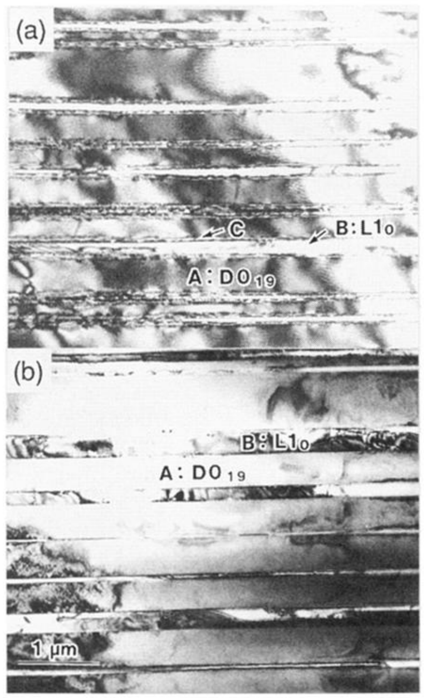

FIG. 1. Bright-field images taken from the samples aged at 1273 K for 2 h (a) and 100 h (b).

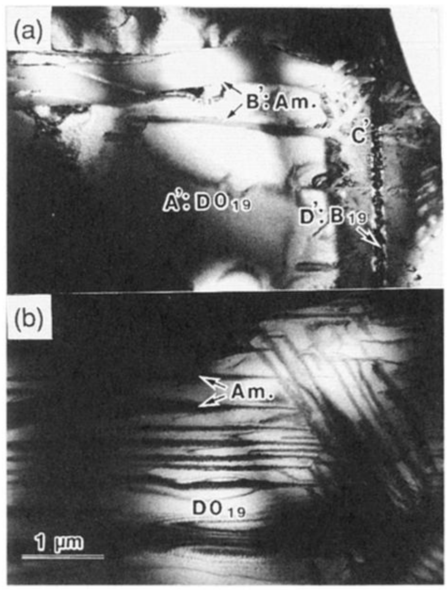

FIG. 2. Bright-field images taken from two different areas of the sample aged at 1273 K for 15 min. In these images, "Am." denotes the amorphous phase.

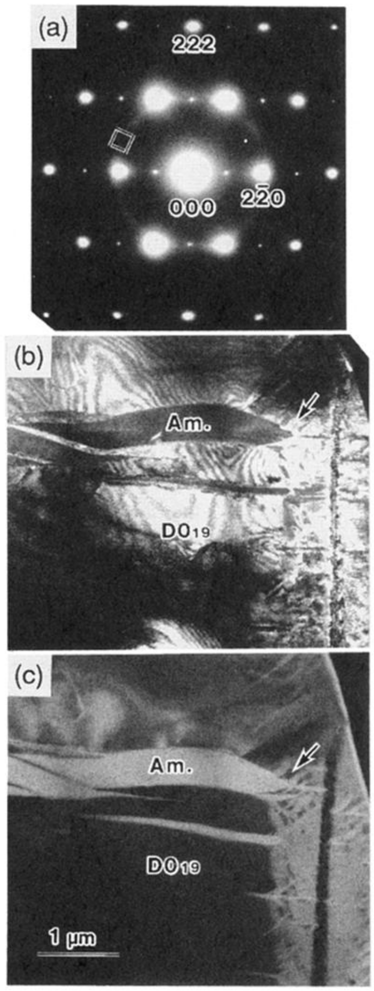

FIG. 3. Electron diffraction pattern (a) and dark-field images (b) and (c), which were obtained from the area shown in Fig. 2(a). In the pattern, diffraction spots are indexed in terms of the $D0_{19}$ structure. The dark-field images were, respectively, taken by using the 222 fundamental spot due to the $D0_{19}$ structure (b), and a part of the first halo ring (c).

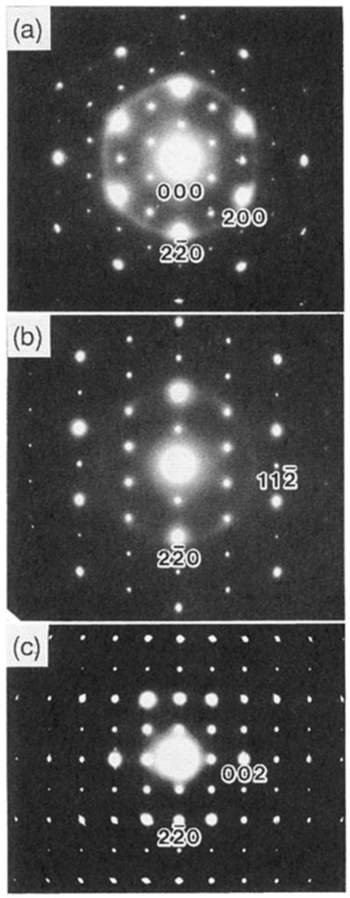

FIG. 4. Electron diffraction patterns taken from the same area in the sample aged for 15 min. The electron incidences are parallel to the $[001]_{\alpha_2}$ (a), $[111]_{\alpha_2}$ (b), and $[110]_{\alpha_2}$ directions (c).

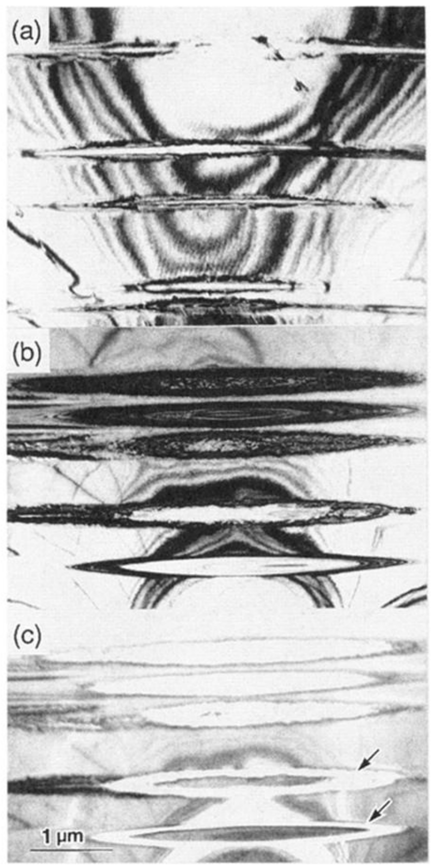

FIG. 5. Bright-field images (a) and (b) and dark-field image (c) of the samples aged for 25 min. Among these images, the two bright-field images were taken from samples made by ion thinning (a) and electropolishing (b). The dark-field image (c) was also taken from the area shown in (b), by using a part of the first halo ring.